CLICdp-Note-2018-004
23 November 2018

Jet Performance at CLIC

Matthias Weber*

* *CERN, Switzerland*

Abstract

In this note the performance of jet reconstruction in e^+e^- collisions at the Compact Linear Collider is studied. The study is based on fully simulated events using the latest version of the CLICdet model. Jet energy and angular resolutions are investigated in di-jet events. The precision with which the detector can measure heavy resonance masses in hadronic decay channels is presented, using the separation power between Z and W di-jet masses as examples. The impact of beam-induced background from $\gamma\gamma \rightarrow$ hadrons on the jet performance is explored.

This work was carried out in the framework of the CLICdp Collaboration

1 Introduction

The Compact Linear Collider (CLIC) is a proposed linear electron-positron collider, which will provide collisions with nominal centre-of-mass energies ranging from 380 GeV to 3 TeV. Final states involving jets are of particular interest at CLIC, e.g. in Higgsstrahlung $e^+e^- \to HZ$, where both H and Z decay predominantly to hadronic final states. Physics backgrounds for these decay channels are produced at a lower relative rate than in hadron-hadron collisions. In order to achieve a precise measurement a good jet energy resolution, which allows for very accurate separation of reconstructed boson mass peaks, is essential. Photons emitted from incoming electron and positron beams can interact and produce additional mini-jets of hadrons. This beam-induced background can be modelled by overlaying these $\gamma\gamma \to$ hadrons collisions on the hard physics event. We will discuss the performance of jets in di-jet events as well as the ability to differentiate between boson mass peaks. The impact of beam-induced backgrounds will be evaluated for beam conditions at 380 GeV and 3 TeV.

2 Jet performance in di-jet events

Di-jet samples from $Z/\gamma^* \to q\bar{q}$, simulated without initial state photon radiation and at several centre-of-mass energies, are used to study the performance of jet reconstruction in CLICdet [1]. These events have an experimental signature of back-to-back, approximately mono-energetic jets. The samples are generated with PYTHIA6.4 [2] and the primary $q\bar{q}$ pairs are limited to light (up, down, and strange) quarks, to reduce the impact of neutrinos in the final state. The software chain uses the DD4hep detector description toolkit [3, 4] and the detector response is simulated using the GEANT4 10.02.p02 toolkit [5]. Software compensation [6] is applied to hadron clusters to improve their energy measurement. Each particle is reconstructed using the Pandora particle flow algorithms [7, 8], combining information from tracks, calorimeter clusters and hits in the muon system. Each type of Pandora particle flow object (PandoraPFO) – charged hadrons, photons, neutral hadrons, electrons, and muons – is calibrated separately with type specific calibration constants. The software packages of iLCSoft-2018-10-11_gcc62 have been used throughout the study with the CLICdet geometry version CLIC_o3_v14.

The jet energy resolution is studied with two methods. The first method compares the energy sum of all reconstructed particles $E_{\text{tot}}^{\text{PFOs}}$ ("detector level") to the sum of all stable visible particles E_{true} [9], excluding neutrinos, without simulation of detector response ("particle level"). Since the vast majority of $Z/\gamma^* \to q\bar{q}$ events is reconstructed in a di-jet signature, this procedure effectively measures the energy resolution of jets with an energy of half the centre-of-mass energy E_{cm}, assuming that all particles are clustered into two jets. The relative energy resolution for a jet energy of $E_j = 1/2 \cdot E_{\text{cm}}$ is then calculated as $\Delta E_j/E_j = \sqrt{2} \cdot \text{RMS}_{90}(E_{\text{tot}}^{\text{PFOs}}/E_{\text{true}})/\text{Mean}_{90}(E_{\text{tot}}^{\text{PFOs}}/E_{\text{true}})$. RMS_{90} is used as a measure of the jet energy resolution. It is defined as the RMS in the smallest range of the distribution containing 90% of the events [8]. The second method compares the response of particle-level jets (clustering stable visible particles, j_G) to those reconstructed at detector level (clustering PandoraPFOs, j_R), using the VLC algorithm [10] as implemented in the FastJet library [11] in exclusive mode to force the event into two jets. The γ and β parameters of VLC are fixed to 1.0 and the radius parameter is set to $R = 0.7$. The VLC algorithm combines a Durham like inter-particle distance $d_{ij} = 2\min(E_i^{2\beta}, E_j^{2\beta})(1-\cos\theta_{ij})/R^2$ based on energy and polar angle with a beam distance $d_{i\text{B}} = E_i^{2\beta}\sin^{2\gamma}\theta_{i\text{B}}$. The algorithm applies a sequential recombination procedure, similar to those present in hadron collider algorithms, providing a robust performance at e^+e^- colliders with non-negligible background. The two reconstructed jets are required to be matched to each of the particle level jets within an angle of 10°.
To illustrate the effectiveness of the exclusive jet clustering algorithm used, Fig. 1 shows the fraction of the visible energy of an event that is contained in two jets at particle level in di-jet signatures. For most events, and for all centre-of-mass energies the amount of unclustered energy is low. The larger the

jet energy, the more collimated the jet. For low energy jets with energies around 50 GeV, the energy distribution within the jet is wider with a larger fraction of the energy distributed away from the jet axis. Thus the peak of the distribution is around 0.97 and a longer tail to lower values is observed. For low energies, larger cones could be of benefit to capture the whole energy of the event, but at the cost of an increased impact from $\gamma\gamma \to$ hadrons backgrounds.

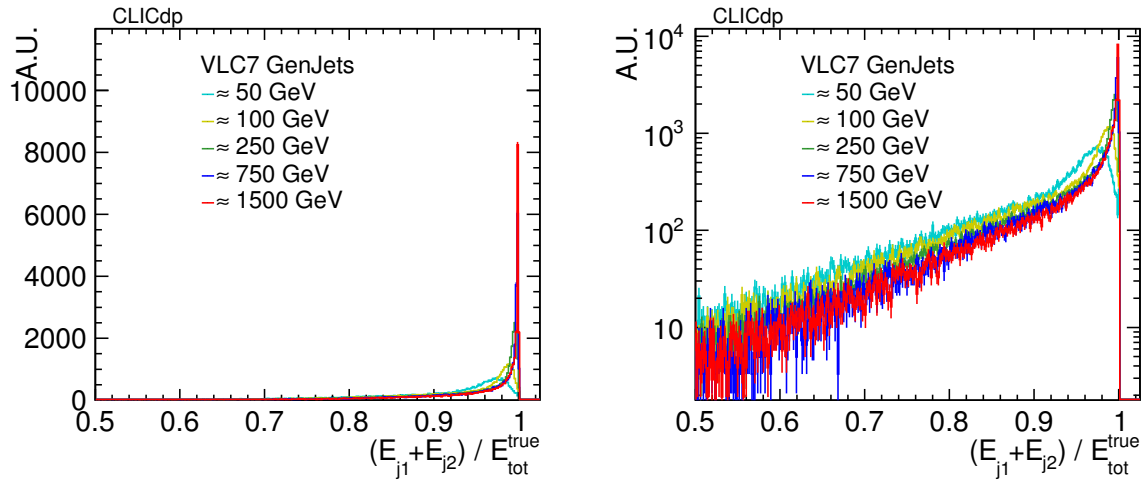

Figure 1: Fraction of the visible energy of a di-jet event contained within two jets, defined by the VLC clustering algorithm with $R = 0.7$ (VLC7), at particle level for different jet energies (left). We display the y-axis in logarithmic scale to emphasise the behaviour for low energy jets (right).

Studies using both methods in di-jet events lead to equivalent values of the jet energy resolution for most of the range as shown in Fig. 2 for several jet energies as function of the quark $|\cos\theta|$. For low energy jets at 50 GeV, the jet energy resolution values are around 4.5–5.5% for barrel ($|\cos\theta| < 0.7$) and endcap jets ($0.80 < |\cos\theta| < 0.925$). For jets beyond 150 GeV, the jet energy resolutions are between 3–4.0% over most of the angular range. For forward jets ($|\cos\theta|$ between 0.925 and 0.975) the jet energy resolutions increase by typically 0.5–2.0% points. For very forward jets ($0.975 < |\cos\theta| < 0.985$), part of the jet can be beyond the tracking volume.

The RMS_{90} result can be compared to results of a fit of the jet energy response with a double sided Crystal ball function [12], using the Minuit2 library [13] as implemented in ROOT 6.08.00 [14]. The procedure starts by fitting a Gaussian over the full range, iteratively changing the fit range until the standard deviation σ of the fit stabilises within 5%. The range of the σ parameter of the Crystal Ball fit is restricted to be within a factor of 2 around the width of the Gaussian fit. Non-Gaussian tails are particularly significant in simulated data that include beam-induced backgrounds from $\gamma\gamma \to$ hadrons and can be modelled by the double-sided Crystal Ball function (see Fig. 3).

Figure 4 compares the resolutions obtained with RMS_{90} and the one from the Crystal Ball σ for different jet energies in events with 3 TeV $\gamma\gamma \to$ hadrons beam-induced background. In events where 3 TeV beam-induced backgrounds from $\gamma\gamma \to$ hadrons are overlaid on the physics event, *tight* [8] selection cuts are applied to the PandoraPFOs prior to jet clustering. These beam-induced backgrounds represent 30 bunch crossings. In general for the jet energy response distributions, the standard deviation σ of the Gaussian core of the double-sided Crystal Ball fits are in good agreement with RMS_{90} values for almost all jet energies and polar angles. The jet energy resolution values are between 3.5–10% for barrel and endcap jets in the presence of 3 TeV backgrounds. For 50 GeV jets, the σ of the fit is considerably lower

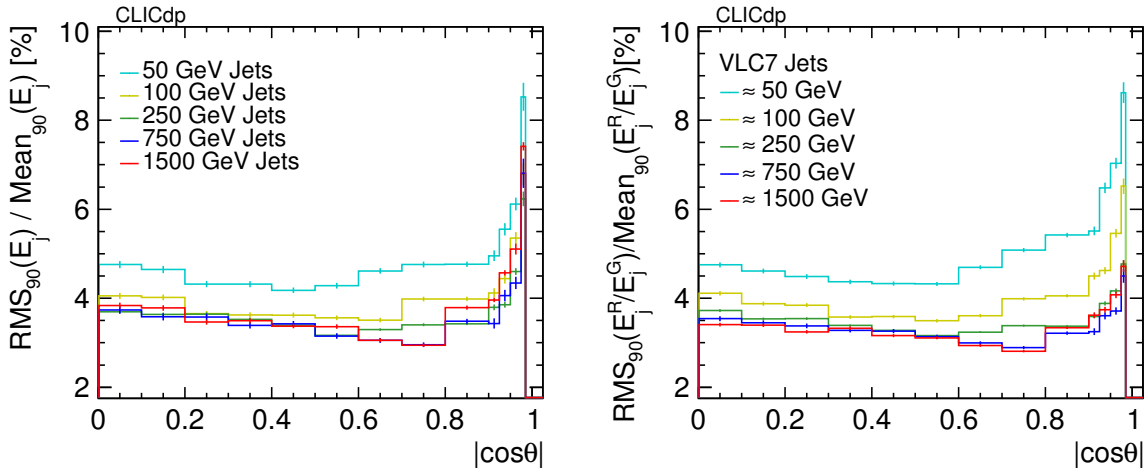

Figure 2: Jet energy resolution distributions for various jet energies as function of $|\cos\theta|$ of the quark using two methods. The first method compares the total reconstructed energy with the energy sum from all visible particles on MC truth (left). The second method compares the jet energy of reconstructed jets and matched MC truth particle jets, using the VLC algorithm with $R = 0.7$ (VLC7, right).

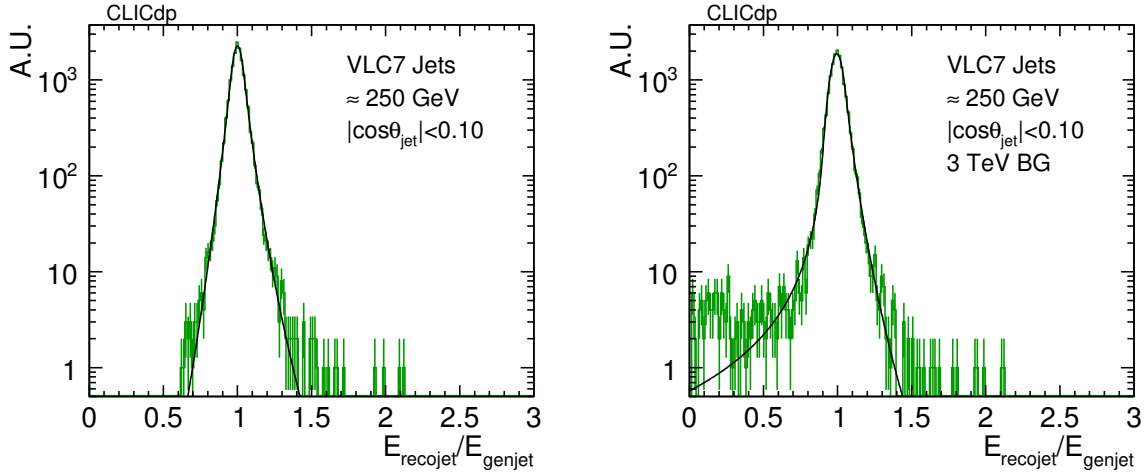

Figure 3: Jet energy resolution for central jets ($|\cos\theta| < 0.10$) of around 250 GeV without (left) and with 3 TeV $\gamma\gamma \to$ hadrons background overlaid (right) on the physics di-jet event, together with corresponding double-sided Crystal Ball fits. Tight PFO selection cuts are used for events with background.

than the RMS_{90} values, where a decrease is observed from 7% to 6% in the detector barrel for events with beam-induced backgrounds. Jet energy resolutions are around 3.5–4.5% for large jet energies beyond 200 GeV, using both measures as quantification. In the forward region ($|\cos\theta|$>0.925) the σ of the fit is below 6% for most jet energies. The beam-induced background leads to larger tails in the jet energy response distribution in this detector region, which are reflected in the larger values of the RMS_{90} measure.

Compared to jet energy resolution values in events without $\gamma\gamma \to$ hadrons backgrounds (Fig. 2), a degradation of the jet energy resolution is observed for all jet energies. The effect is most pronounced for low energy jets, e.g. for 50 GeV jets, where the increase is from around 4.5% to 7.5%. For high energy jets,

the jet energy resolution increase is limited to less than 0.5% points for most of the $|\cos\theta|$ range. Since hadrons from beam-induced backgrounds tend to be produced more in the forward direction, their impact is larger for endcap and forward jets than for barrel jets. For low energy jets the jet energy resolution values are significantly better than those obtained by ATLAS [15] and CMS [16].

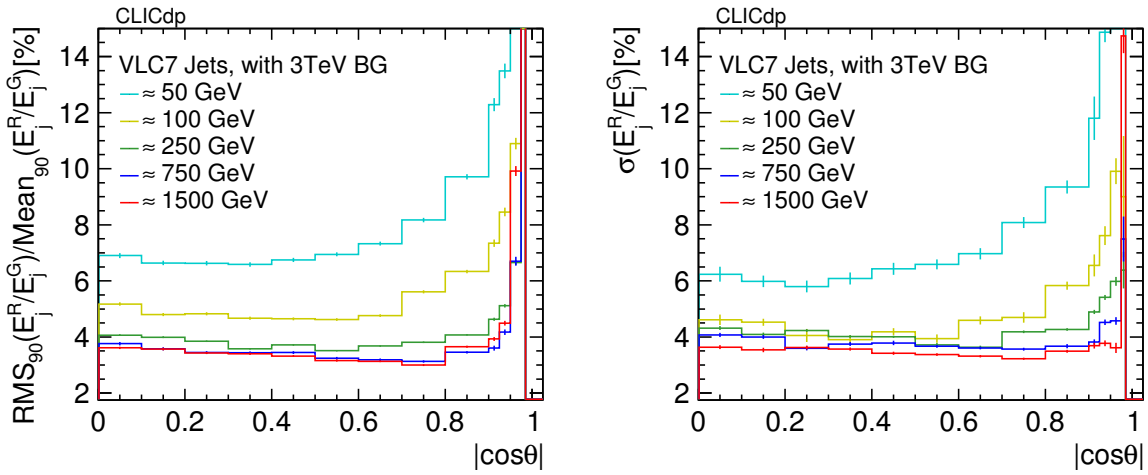

Figure 4: Jet energy resolution for various jet energies as function of $|\cos\theta|$ of the quark with 3 TeV $\gamma\gamma \to$ hadrons background overlaid on the physics di-jet event. In the first figure RMS_{90} is used as measure of the jet energy resolution (left), the standard deviation σ of the Gaussian core of the double-sided Crystal Ball fit quantifies the jet energy resolution in the second figure (right). Tight PFO selection cuts are used.

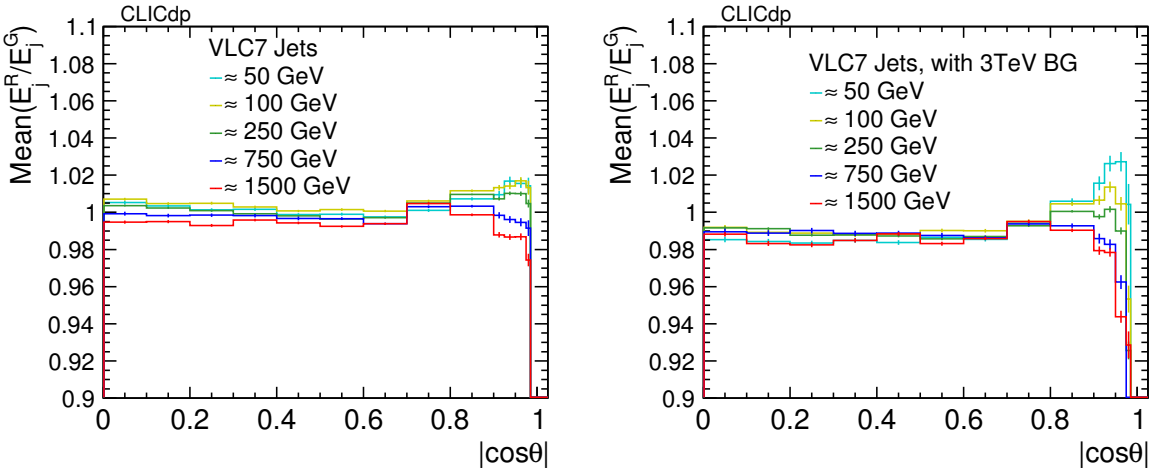

Figure 5: Mean of the jet energy response between the reconstructed and the matched MC truth particle jet for events without (left) and with overlay of 3 TeV beam-induced backgrounds from $\gamma\gamma \to$ hadrons (right). Tight PFO selection cuts are used for events with background.

The mean of the jet energy response histogram $E_j^{\mathrm{R}}/E_j^{\mathrm{G}}$ between the reconstructed and the matched MC truth particle jet is shown in Fig. 5 for events without beam-induced backgrounds and with 3 TeV beam-induced background conditions. In both cases the PandoraPFOs are calibrated, but no further calibration is applied after the jet clustering of the particle flow candidates. For most of detector range the

raw jet energy response is within 1.5% of unity even including $\gamma\gamma \to$ hadrons backgrounds. For jets in the outer endcap ($|\cos\theta| > 0.925$) and in the forward region, where beam-induced backgrounds are more prominent, we observe larger deviations of up to 8%.
The impact of beam-induced backgrounds from $\gamma\gamma \to$ hadrons for the 380 GeV accelerator conditions is evaluated, representing 30 bunch crossings. In events with overlay of 380 GeV beam-backgrounds from $\gamma\gamma \to$ hadrons, *low energy loose* selection cuts [17] are placed on PandoraPFOs, in order to reflect the lower beam-induced backgrounds of the 380 GeV accelerator relative to the 3 TeV accelerator. The impact of 380 GeV beam-induced backgrounds on the jet energy resolution is illustrated by Fig. 6. For jet energies above 100 GeV, the 380 GeV beam-induced background levels lead to almost no increase of the jet energy resolution for barrel and endcap jets, around 0.5–1.0% points can be observed for forward jets. Even for 50 GeV jets in the barrel, only a mild increase of the jet energy resolution to about 5% is obtained. In the outermost part of the barrel and endcaps the jet energy resolution for 50 GeV jets is increased to about 5.5-6.0%. The increase is around 2% points and more for forward jets.

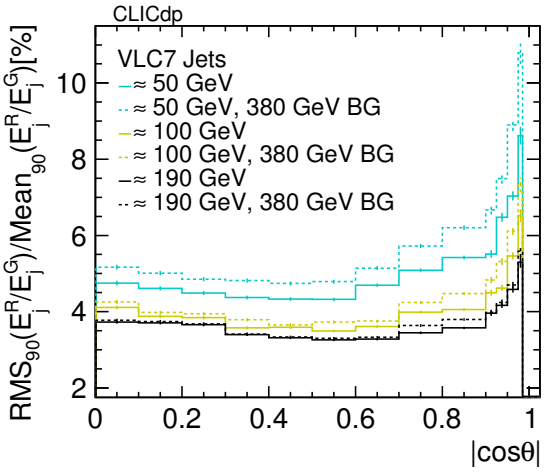

Figure 6: Jet energy resolution for various jet energies as function of $|\cos\theta|$ of the quark with and without 380 GeV $\gamma\gamma \to$ hadrons background overlay on the physics di-jet event. RMS_{90} is used as measure of the jet energy resolution. Low energy loose PFO selection cuts are used for events with background.

The jet angular resolutions in azimuth ϕ and polar angle θ are studied as function of jet energies for different regions in polar angle. For events having significant final state gluon radiation, three jets reflect the event topology better than two jets. Since the jet algorithm is run in exclusive mode with two jets, this can lead to a significant bias in jet angular resolutions. In order to diminish the impact of this bias, we preselect events, where the two particle level MC truth jets are back-to-back in azimuth $\Delta\phi(\mathrm{j1,j2}) > 2.8$ (around 160°), which vetoes against underlying multi-jet topologies. Each of the reconstructed jets is matched to its closest MC truth particle level jet. Figure 7 shows ϕ and θ resolutions using barrel 250 GeV jets with 3 TeV beam-induced backgrounds from $\gamma\gamma \to$ hadrons overlaid, clustered with the VLC algorithm with radius $R = 0.7$. In addition double-sided Crystal Ball fits of the resolution distributions are displayed, showing that the tails are reproduced by the fit. The tails of both distributions reach to about 25°.

The distribution of ϕ resolutions as a function of polar angle, and as a function of jet energy are shown in Fig. 8 in events with 3 TeV beam-induced backgrounds from $\gamma\gamma \to$ hadrons. The more forward the jets, the wider the ϕ resolution distribution. Low energy jets tend to be less collimated and the ϕ resolution

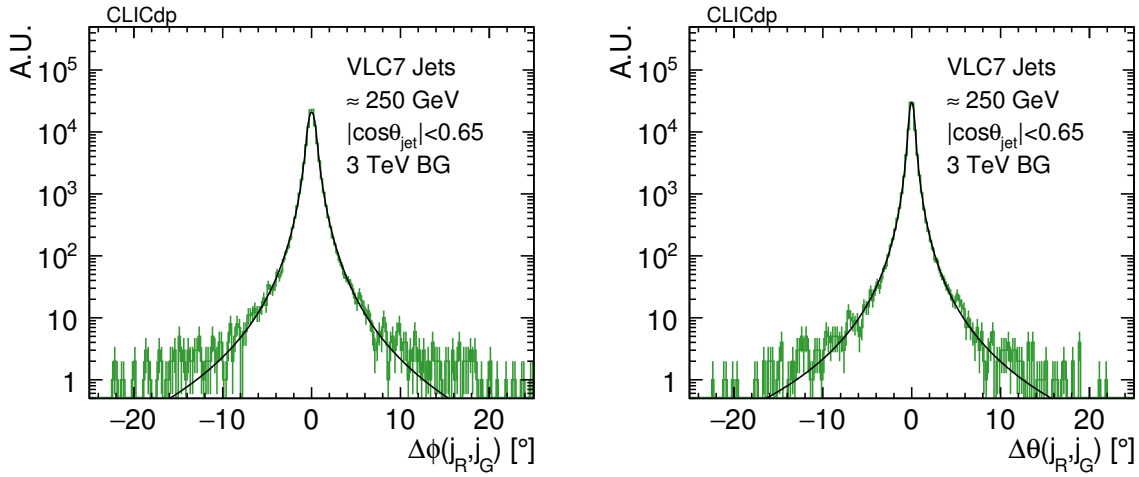

Figure 7: Jet ϕ (left) and θ (right) resolution distributions for barrel jets $|\cos\theta| < 0.65$ with jet energies around 250 GeV, with $\gamma\gamma \to$ hadrons backgrounds at 3 TeV on the physics di-jet event, using tight PFO selection cuts.

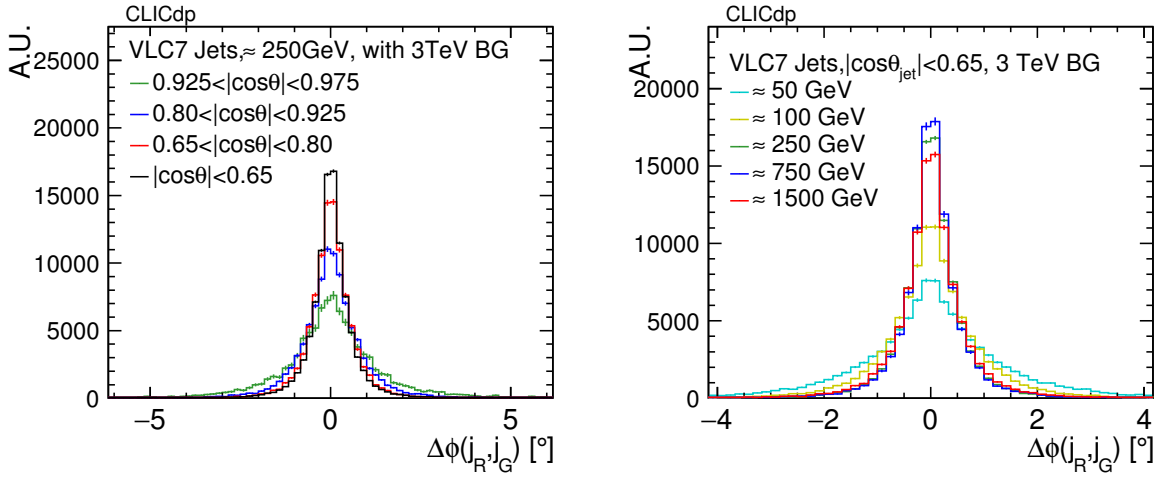

Figure 8: Jet ϕ resolution distributions of 250 GeV jets for various polar angle intervals (left) and jet ϕ resolutions for barrel jets at various jet energies (right), with $\gamma\gamma \to$ hadrons background conditions at 3 TeV and using tight PFO selection cuts.

distribution is wider than for high energy, more collimated jets. The detector is divided into four regions of $|\cos\theta|$: the barrel, the transition region (where the jet energy is reconstructed both in barrel and endcap parts of the detector), the endcap, and the forward region. Fig. 9 shows jet ϕ and θ resolutions. The values are around 0.5% in the barrel, and below 1% in almost all regions for all energies. Jet θ resolutions are slightly better than jet ϕ resolutions with less variation as a function of polar angle. Once beam-induced backgrounds from $\gamma\gamma \to$ hadrons are overlaid, the θ resolutions increase for 50 GeV jets from 0.5 to about 1.0° (see Fig. 10), while for the remaining jet energies the θ resolutions remain around 0.5°. A slight increase in angular resolution for more forward jets can be observed. For jet ϕ resolutions in the barrel region and for most jet energies, the values remain at a similar level of $0.4-0.7^\circ$; for more forward jets and for all energies, the ϕ resolutions increase relatively by around 25–50%. Using the standard deviation σ of the Gaussian core of a double-sided Crystal Ball fit, the values for the jet angular resolutions are lower compared to RMS_{90} values, since the sizeable tails have less impact. This effect is

particularly large for low energy jets and in the forward region of the detector as shown in Fig. 11.

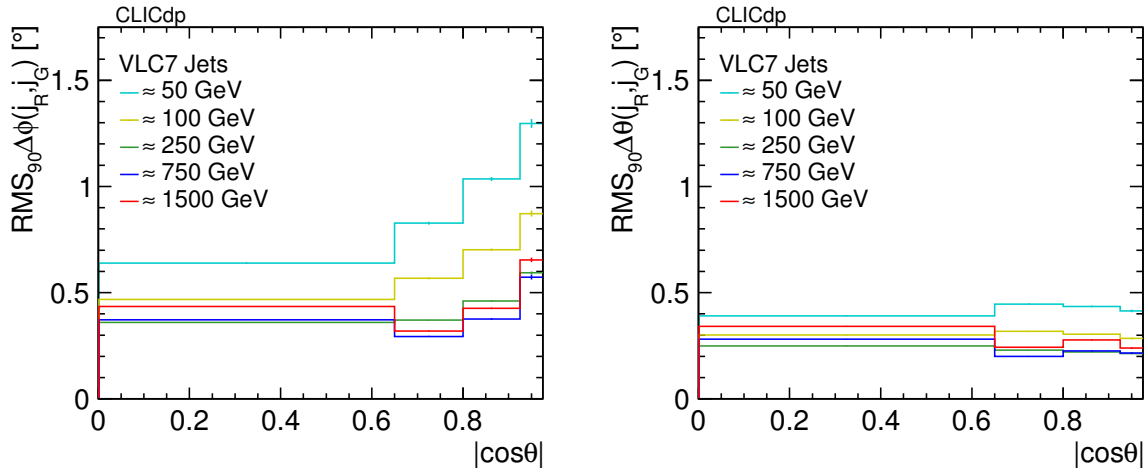

Figure 9: Jet ϕ (left) and θ (right) resolutions for several jet energies in four $|\cos\theta|$ bins in events without any simulation of beam-induced background effects.

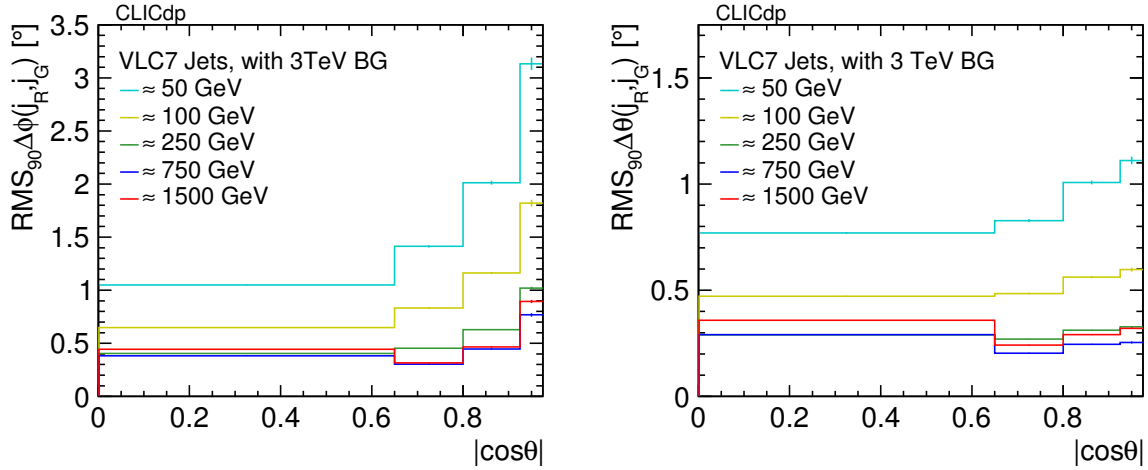

Figure 10: Jet ϕ (left) and θ (right) resolutions for several jet energies in four $|\cos\theta|$ bins in events with 3 TeV beam-induced backgrounds from $\gamma\gamma \to$ hadrons, using tight PFO selection cuts.

3 W and Z mass separation

The precise reconstruction of masses of resonances in hadronic channels over wide ranges of energies is a challenging task. The ability to separate di-jet masses from hadronic decays of W and Z bosons is studied using the Pandora reconstruction algorithms. The study is carried out using simulated di-boson events, in which only one of the bosons decays into di-quarks, i.e. $ZZ \to \nu\bar{\nu}q\bar{q}$ and $WW \to l\nu qq$ with q=u,d,s. The boson energies in this study vary from 125 GeV, where both bosons are created almost at rest, up to 1 TeV, where the bosons are heavily boosted. For each vector boson energy, samples were produced without background (no BG) and with 3 TeV beam-induced backgrounds from $\gamma\gamma \to$ hadrons, representing 30 bunch crossings (3 TeV BG). For low energy bosons of 125 GeV we also investigate the

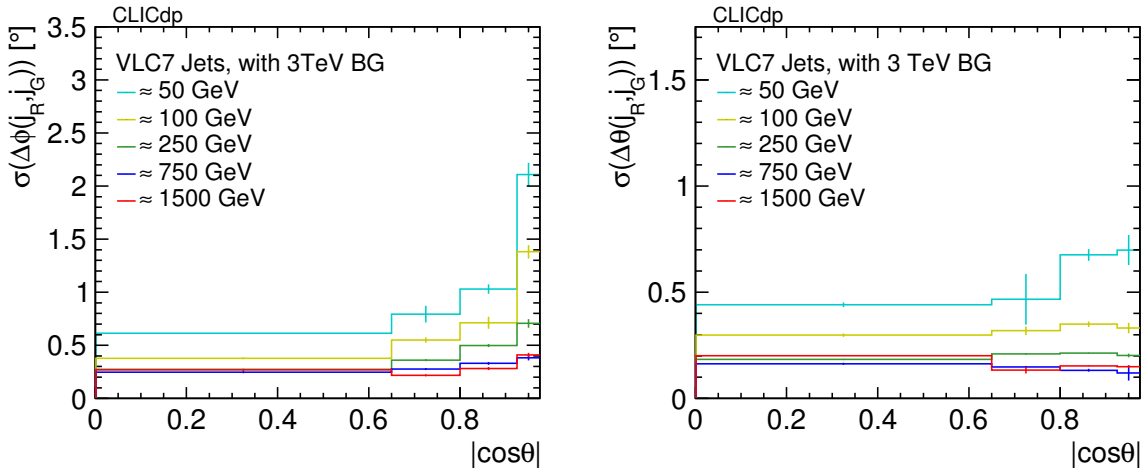

Figure 11: Jet ϕ (left) and θ (right) resolutions for several jet energies in four $|\cos\theta|$ bins in events with 3 TeV beam-induced backgrounds from $\gamma\gamma \to$ hadrons, using tight PFO selection cuts. The standard deviation σ of a double-sided Crystal Ball fit is used as measure for the jet position resolution.

impact of 380 GeV beam-induced backgrounds. Events are reconstructed using the VLC algorithm with parameters $R = 0.7$, $\gamma = \beta$=1 in exclusive mode, forcing the event into two jets. Prior to jet clustering at particle level, the true charged lepton from the W is removed (together with any associated photons from final state radiation and Bremsstrahlung). At detector level, all reconstructed particles within a cone of $|\cos\alpha| < 0.9$ around the true lepton direction are removed prior to jet clustering. This procedure has virtually no impact on particles from the hadronically decaying W. At particle level, visible stable particles are used as input for the jet clustering. On the reconstruction level for the samples without beam-induced backgrounds, all Pandora particle flow objects are used as input for the jet clustering, while tight (low energy loose) selected Pandora particle flow objects are used in the samples including 3 TeV (380 GeV) beam-induced backgrounds. In order to ensure that the event is well contained within the detector acceptance, a cut is imposed on the polar angle of both MC truth jets, $|\cos\theta| < 0.9$.

The di-jet mass distributions have a long tail to low values, as shown in Fig. 12 (left) for low energy bosons. This tail is present at both detector and MC particle level. In these events a sizeable amount of the hadronic energy is not contained in the two jets. In this lower di-jet mass tail, the di-jet momentum is not back-to-back in azimuth with the missing transverse energy vector for Z events (respectively the di-neutrino vector), or the combined vector from missing energy and the lepton direction for W events (respectively the neutrino-lepton vector), both for particle-level jets and detector-level jets (without beam-induced backgrounds). The additional hard radiation is effectively ignored when forcing the event into two jets, and an exclusive three jet reconstruction is more suitable in those events. A requirement on the amount of hadronic energy contained among the leading two jets at particle level of 90% removes this lower di-jet mass tail to a large extent as Fig. 12 (right) shows. For high energy bosons ($E \geq 500\,\text{GeV}$) this requirement removes less than 1% of all events and 6.7% for 250 GeV bosons.

The upper tail and the core of the di-jet mass distribution is described well by a Gaussian function even without this additional preselection criteria for all energies. The di-jet distributions are fitted with a Gaussian, iteratively changing the upper limit of the fit range to mean $+ 2\sigma$ and the lower fit limit to mean $- 2\sigma$ (-1σ without the preselection criteria on the unclustered energy ratio for 125 GeV bosons), until the fitted σ stabilises within 5%. Figure 13 shows the di-jet mass distributions for W and Z bosons

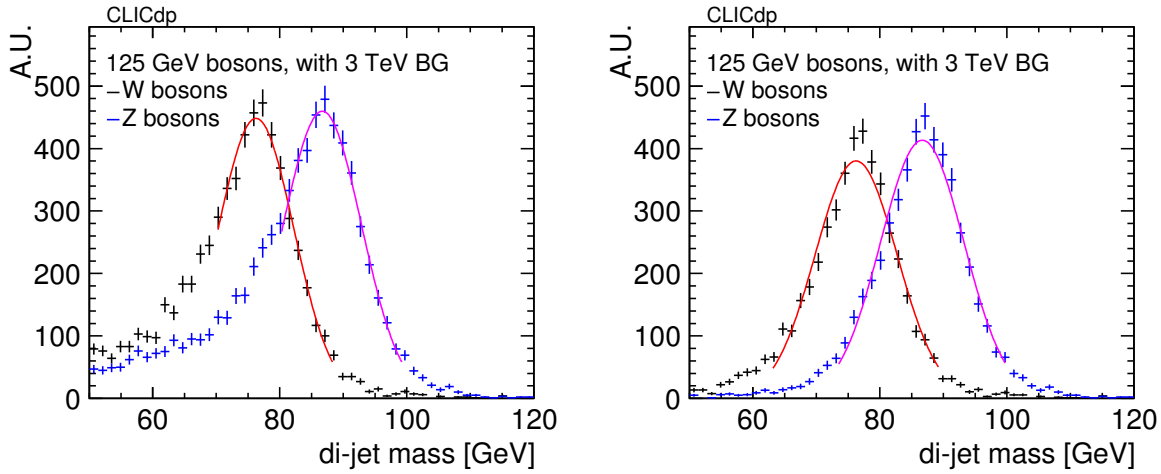

Figure 12: Di-jet mass distributions of hadronically decaying W and Z with $E = 125\,\text{GeV}$ in $\text{WW} \to l\nu qq$ and $\text{ZZ} \to \nu\bar{\nu}q\bar{q}$ events, together with Gaussian fits of the di-jet mass peak (left). An additional preselection cut has been placed on the amount of hadronic energy clustered within the leading two jets at particle level larger than 90% in order to remove multi-jet signatures (right). The events include 3 TeV beam-induced backgrounds from $\gamma\gamma \to$ hadrons and tight PFO selection cuts are used.

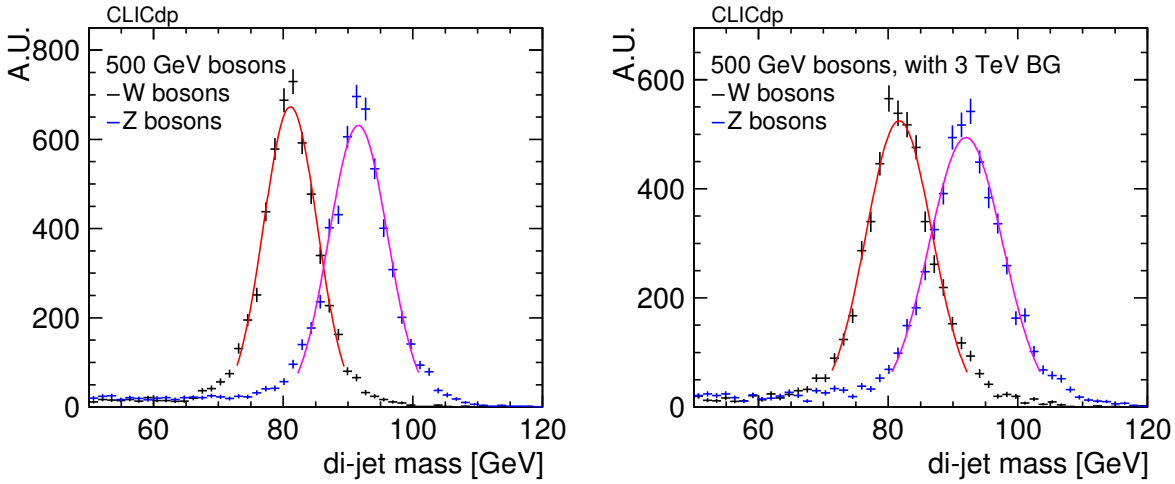

Figure 13: Di-jet mass distributions of hadronically decaying W and Z with $E = 500\,\text{GeV}$ in $\text{WW} \to l\nu qq$ and $\text{ZZ} \to \nu\bar{\nu}q\bar{q}$ events, together with Gaussian fits of the di-jet mass for events without beam-induced backgrounds (right) and overlay of 3 TeV beam-induced backgrounds from $\gamma\gamma \to$ hadrons (left). Tight PFO selection cuts are used for events with background.

with $E = 500\,\text{GeV}$ with the Gaussian fits in events without and with the simulation of 3 TeV beam-induced backgrounds from $\gamma\gamma \to$ hadrons.

Since the di-jet mass distributions are not further calibrated at the moment, we shift the mean of the fit to the W and Z masses, fixing the ratio of σ/mean. The rescaled Gaussian distributions are normalised, such that integral of the distributions is 1. The overlap fraction A_O is defined by

$$A_\text{O} = \left(\int_{-\infty}^{x_\text{int}} \text{gauss}_\text{Z}(x)\text{dx} + \int_{x_\text{int}}^{\infty} \text{gauss}_\text{W}(x)\text{dx} \right) /2,$$

where x_{int} is the intersection mass point of the Gaussian fit of the W and Z di-jet mass distributions between the W and Z masses. The efficiency ε of selecting W's or Z's are represented by the integrals of the Gaussian curves up to x_{int} for W's and from x_{int} onwards for Z's. The ideal Gaussian separation is evaluated using the quantile function with the normal distribution[1]. A different approach using the average mass resolution $\sigma_{\text{avg}} = (\sigma_{\text{Z}} + \sigma_{\text{W}})/2$ found the same results for the separation $\mathscr{S} = (m_{\text{Z}} - m_{\text{W}})/\sigma_{\text{avg}}$.

Table 1: Mass resolutions, selection efficiencies, and separation of W and Z peaks for reconstructed W and Z's at different energies, with and without overlaid beam-induced backgrounds from $\gamma\gamma \to$ hadrons. Tight PFO (Low energy loose) selection cuts are used for events with 3 TeV (380 GeV) background:

Background	$E_{\text{W,Z}}$ [GeV]	$\sigma_{m(\text{W})}/m(\text{W})$ [%]	$\sigma_{m(\text{Z})}/m(\text{Z})$ [%]	ε [%]	Separation [σ]
no BG	125	5.5	5.3	88	2.3
	250	5.3	5.4	88	2.3
	500	5.1	4.9	90	2.5
	1000	6.6	6.2	84	2.0
3 TeV BG	125	7.8	7.1	80	1.7
	250	6.9	6.8	82	1.8
	500	6.2	6.1	85	2.0
	1000	7.9	7.2	80	1.7
380 GeV BG	125	6.0	5.5	87	2.2

The di-jet mass resolutions are listed in Table 1, together with identification efficiencies and the separation between W and Z peaks. In events without beam-induced background effects the selection efficiency is between 84% and 90%, which corresponds to an overlap fraction of 10–16%. For very boosted bosons the mass resolution is slightly worse than for bosons at rest or with moderate energies. Once 3 TeV beam-induced backgrounds from $\gamma\gamma \to$ hadrons are taken into account, the W and Z selection efficiencies decrease to 80–85%, which corresponds to overlap fractions of 15–20%. The degradation is worse for lower boson energies. The peak separation diminishes from 2.0–2.5 σ to about 1.7–2.0 σ in the presence of beam-induced background levels of the 3 TeV accelerator. As alternatives, no selection, loose selection and medium selection criteria have been applied to PandoraPFOs prior to jet clustering in simulated events with 3 TeV beam-induced backgrounds. These three alternative selections led to wider di-jet mass distributions and a diminished separation power between the two mass peaks. For 380 GeV beam-induced background levels there is a mild effect on the separation power, decreasing from 2.3 σ to 2.2 σ.

4 Summary

The performance of jets at CLIC has been studied in di-jet events, using the latest detector model CLICdet and the new software chain. Using RMS_{90} to quantify the jet energy resolution, relative jet energy resolution values of typically 4–5% are obtained for jets of energies between 50 GeV and 1.5 TeV in barrel and endcap regions, with slightly larger jet energy resolutions for forward jets. Once beam-induced backgrounds from $\gamma\gamma \to$ hadrons as expected for 3 TeV collisions are overlaid, the jet energy resolution

[1] separation calculation using ROOT 6.08.00: $\mathscr{S} = 2 \cdot |\text{ROOT :: Math :: normal\_quantile}(A_{\text{O}}, 1)|$

for low energy jets increases to about 6–8%. The impact of beam-induced background on jets with energies beyond 200 GeV increases the jet energy resolution by additional 0.5% points. The quantitative results for the jet energy resolutions are very similar for two estimators considered: the σ of the Gaussian core of a double-sided Crystal Ball function or RMS_{90}. For 380 GeV beam-induced background conditions, the jet energy resolutions are considerably less affected compared to 3 TeV conditions, adding only 0.5% points even for 50 GeV jets. Jet polar angle θ resolutions are typically lower than 1° and jet azimuthal angle ϕ resolutions are within 1.5° for all jet energies studied and all detector regions, even taking into account beam-induced backgrounds levels of the 3 TeV collider from $\gamma\gamma \rightarrow$ hadrons. The ability to distinguish between masses of resonances was investigated using hadronically decaying W and Z bosons. For boson energies between 125 and 1000 GeV, a peak separation of 1.7–2.0 σ was achieved in events with 3 TeV beam-induced backgrounds.

Acknowledgements

This project has received funding from the European Union's Horizon 2020 Research and Innovation programme under Grant Agreement no. 654168.

References

[1] N. Alipour Tehrani et al., *CLICdet: The post-CDR CLIC detector model* (2017), URL: https://cds.cern.ch/record/2254048.

[2] T. Sjöstrand, S. Mrenna, P. Skands, *PYTHIA 6.4 physics and manual*, JHEP **05** (2006) 026, arXiv: 0603175 [hep-ph].

[3] M. Petric et al., *Detector simulations with DD4hep*, J. Phys. Conf. Ser. **898** (2017) 042015, DOI: 10.1088/1742-6596/898/4/042015.

[4] A. Sailer et al., ILD, CLICdp, *DD4Hep based event reconstruction*, J. Phys. Conf. Ser. **898** (2017) 042017, DOI: 10.1088/1742-6596/898/4/042017.

[5] S. Agostinelli et al., *Geant4 – A Simulation Toolkit*, Nucl. Instrum. Methods A **506** (2003) 250, DOI: 10.1016/S0168-9002(03)01368-8.

[6] H. Tran et al., *Software compensation in Particle Flow reconstruction*, Eur. Phys. J. **C77** (2017) 698, DOI: 10.1140/epjc/s10052-017-5298-3, arXiv: 1705.10363 [physics.ins-det].

[7] J. Marshall, M. Thomson, *The Pandora Software Development Kit for Pattern Recognition*, Eur.Phys.J. **C75** (2015) 439, DOI: 10.1140/epjc/s10052-015-3659-3, arXiv: 1506.05348 [physics.data-an].

[8] J. S. Marshall, A. Münnich, M. Thomson, *Performance of Particle Flow Calorimetry at CLIC*, Nucl. Instrum. Meth. **A700** (2013) 153, DOI: 10.1016/j.nima.2012.10.038, arXiv: 1209.4039 [physics.ins-det].

[9] C. Buttar et al., *Standard Model Handles and Candles Working Group: Tools and Jets Summary Report*, Physics at TeV colliders, La physique du TeV aux collisionneurs, Les Houches 2007 : 11-29 June 2007, 2008, p. 121, arXiv: 0803.0678 [hep-ph], URL: https://inspirehep.net/record/780755/files/arXiv:0803.0678.pdf.

[10] M. Boronat et al., *Jet reconstruction at high-energy electron-positron colliders*, Eur. Phys. J. **C78** (2018) 144, DOI: 10.1140/epjc/s10052-018-5594-6, arXiv: 1607.05039 [hep-ex].

[11] M. Cacciari, G. P. Salam, G. Soyez, *FastJet User Manual*, Eur. Phys. J. **C72** (2012) 1896, DOI: 10.1140/epjc/s10052-012-1896-2, arXiv: 1111.6097 [hep-ph].

[12] M. Oreglia, *A Study of the Reactions $\psi' \to \gamma\gamma\psi$*, PhD thesis, SLAC, 1980, URL: http://www-public.slac.stanford.edu/sciDoc/docMeta.aspx?slacPubNumber=slac-r-236.html.

[13] F. James, *MINUIT Function Minimization and Error Analysis: Reference Manual Version 94.1* (1994).

[14] I. Antcheva et al., *ROOT: A C++ framework for petabyte data storage, statistical analysis and visualization*, Comput. Phys. Commun. **180** (2009) 2499, DOI: 10.1016/j.cpc.2009.08.005, arXiv: 1508.07749 [physics.data-an].

[15] M. Aaboud et al., ATLAS, *Jet reconstruction and performance using particle flow with the ATLAS Detector*, Eur. Phys. J. **C77** (2017) 466, DOI: 10.1140/epjc/s10052-017-5031-2, arXiv: 1703.10485 [hep-ex].

[16] V. Khachatryan et al., CMS,
Jet energy scale and resolution in the CMS experiment in pp collisions at 8 TeV,
JINST **12** (2017) P02014, DOI: 10.1088/1748-0221/12/02/P02014,
arXiv: 1607.03663 [hep-ex].

[17] E. Brondolin, A. Sailer, *Optimization of timing selections at 380 GeV CLIC* (2018),
arXiv: 1811.00466 [hep-ex].